LED-pump-X-ray-multiprobe Crystallography for Sub-second Timescales

Paul Raithby (p.r.raithby@bath.ac.uk)
University of Bath https://orcid.org/0000-0002-2944-0662
Lauren Hatcher
Cardiff University
Mark Warren
Diamond Light Source
Jonathan Skelton
University of Manchester
Anuradha Pallipurath
University of Leeds
Lucy Saunders
Diamond Light Source https://orcid.org/0000-0001-5689-8129
David Allan
Diamond Light Source
Paul Hathaway
Diamond Light Source
Guilio Crevatin
Diamond Light Source
David Omar
Diamond Light Source
Benjamin Williams
Diamond Light Source https://orcid.org/0000-0001-9544-0890
Chick Wilson
University of Bath

Article

Keywords:

Posted Date: January 24th, 2022

DOI: https://doi.org/10.21203/rs.3.rs-1253485/v1

Version of Record: A version of this preprint was published at Communications Chemistry on August 26th, 2022. See the published version at https://doi.org/10.1038/s42004-022-00716-1.

LED-pump-X-ray-multiprobe crystallography for sub-second timescales

L. E. Hatcher,[1,2] M. R. Warren,[3] J. M. Skelton,[1,4] A. R. Pallipurath,[1,5] L. K. Saunders,[3] D. R. Allan,[3] P. Hathaway,[3] G. Crevatin,[3] D. Omar,[3] B. H. Williams,[3] C. C. Wilson[1] and P. R. Raithby[1]*

[1] Department of Chemistry, University of Bath, Bath, UK.

[2] School of Chemistry, Cardiff University, Cardiff, UK.

[3] Diamond Light Source, Harwell Science and Innovation Campus, Didcot, UK.

[4] Department of Chemistry, University of Manchester, Manchester, UK.

[5] School of Chemical and Process Engineering, University of Leeds, Leeds, UK.

* E-mail: p.r.raithby@bath.ac.uk

Abstract

We present a pump-multiprobe single-crystal X-ray diffraction (SCXRD) technique for studying photoexcited solid-state species with millisecond-to-minute lifetimes. We excite using pulsed LEDs and synchronise to a gated X-ray detector to collect 3D structures with sub-second time resolution while maximising photo-conversion and minimising beam damage. Our implementation provides complete control of the pump-multiprobe sequencing and can access a range of timescales using the same setup. Using LEDs allows variation of the intensity and pulse width and ensures uniform illumination of the crystal, spreading the energy load in time and space. We demonstrate our method by studying the variable-temperature kinetics of photo-activated linkage isomerism in [Pd(Bu$_4$dien)(NO$_2$)][BPh$_4$] single-crystals. We further show that our method extends to following indicative Bragg reflections with a continuous readout Timepix3 detector chip. Our approach is applicable to a range of physical and biological processes that occur on millisecond and slower timescales, which cannot be studied using existing techniques.

The ability to monitor solid-state reactions in real-time contributes enormously to our understanding of structure-function relationships and assists in designing new materials. The ability to watch chemical and biological processes in 3D, and as they occur, opens up new vistas of chemical research.

SCXRD provides complete 3D structures and is the "gold standard" for studying solid-state processes in single-crystals.[1] Photocrystallography experiments, where molecules in a crystal are activated by light and the structural changes observed using diffraction, have been successfully used to study various light-induced reactions.[2-4] However, diffraction datasets are inherently time-averaged and initial photocrystallographic experiments were limited to timescales of minutes to hours and hence to starting materials or photo-products. Over the last two decades, the advent of fast pulsed lasers, reliable cryogenics, bright synchrotron sources and, most recently, X-ray free-electron lasers (XFELs), have made it possible to study transient species with lifetimes from milliseconds to femtoseconds.[5, 6]

The state-of-the-art for time-resolved measurements on macromolecules is Laue diffraction, with synchrotron sources allowing characterization of species with lifetimes down to ~1 ps using streak cameras and bunch-slicing,[7, 8] and to femtoseconds at XFELs.[5, 9, 10] However, solving structures from Laue diffraction is challenging and typically requires a good starting model, making it difficult to identify unknown intermediates. Excepting a handful of examples using Laue methods to study species with microsecond lifetimes,[11-13] molecular crystallography has therefore continued to use monochromatic X-rays, despite flux limitations.[14-18]

Pump-probe photocrystallography experiments are also constrained by the excitation source. Experiments typically synchronise the X-ray beam or a gated detector to a pulsed laser with nanosecond to femtosecond pulse-widths. The timing sequence is then dictated by the laser repetition rate, and high-flux X-rays are required to collect measurable diffraction data between pulses. Short, high-intensity laser pulses can lead to photo-bleaching, low photoexcitation levels, sample heating and uneven illumination. Exposure to high-intensity light and/or X-rays can cause rapid crystal damage,[19, 20] while high-flux X-rays can also induce excitation.[21, 22]

Previous time-resolved SCXRD experiments have largely focussed on microsecond and shorter lifetimes, due to the availability of lasers operating on these timescales and the pursuit of ever-faster time-resolution. Consequently, there are comparatively few methods suited to lifetimes of minutes to milliseconds. This is despite the many interesting physical and biological transformations occurring on these timescales, including protein folding, ligand binding, phase transitions, crystal nucleation and X-ray-induced crystal damage.[6, 19, 23-26] Some recent studies have investigated millisecond kinetics using gated X-ray detectors to follow selected Bragg reflections,[27] but this is insufficient to solve 3D structures and therefore cannot unambiguously identify unknown intermediates.

The latest developments in synchrotron sources and gated photon-counting detectors provide an opportunity to address the limitations of existing time-resolved SCXRD methods and obtain complete datasets with sub-second time-resolution. We have developed a new LED-pump-X-ray-multiprobe technique for studying single-crystal photoswitching at minute to millisecond timescales. Our method enables collection of high-quality SCXRD datasets considerably faster than previous pump-probe methods,[15, 16] while using a pulsed LED pump ensures uniform sample illumination and allows the pump-multiprobe timing sequence and the excitation pulse-width and intensity to be straightforwardly tuned to maximise photoexcitation and minimise crystal damage. This delivers higher excited-state (ES) populations than in traditional laser experiments, enabling the 3D structure of unknown species to be solved without an initial model. We have applied our technique to study the photo-activated $NO_2 \rightarrow ONO$ linkage isomerism in $[Pd(Bu_4dien)(NO_2)][BPh_4]$ (**1**, Bu_4dien = *N,N,N',N'*-tetrabutyldiethylenetriamine, BPh_4 = tetraphenylborate).[6] We obtain new insight into the photoexcitation at close-to-ambient temperature and visualise changes in electron-density on irradiation as a time-resolved "molecular movie" with 400 ms resolution.

This methodology can be adapted to study a variety of molecular/macromolecular processes and may be paired with techniques such as HATRX to improve the signal-to-noise ratio and/or access even faster timescales.[28]

Results

Model system. Our method was developed against the model linkage isomer crystal **1**. **1** photoexcites from a ground-state (GS) nitro-(η^1-NO_2) to an ES *endo*-nitrito-(η^1-ONO) isomer with 100% conversion.[29] The reverse ONO→NO_2 process is thermally-induced and the ES lifetime is strongly temperature-dependent.[30] This makes **1** an ideal test system for time-resolved SCXRD methods, as the ES lifetime can be straightforwardly matched to the measurement timescale by selecting an appropriate temperature. Preliminary experiments to confirm the response of the crystal in the experiment set-up were performed as previously described.[30]

Pump-multiprobe data collection strategy. The light-pump used was a bespoke pulsed LED array (Figures 1(a)/(b)). A typical pump-probe sequence with duration $t_{\mathrm{cyc}} = t_{\mathrm{exc}} + t_{\mathrm{dec}}$, where the pump is on for an excitation time t_{exc} and off for a decay time t_{dec}, is shown in Figure 1(c). A major challenge in time-resolved SCXRD experiments is designing a data-collection strategy that provides complete X-ray datasets, allowing for full structural determination, within a reasonable overall experiment time. To obtain accurate intensities each reflection needs to be sampled multiple times across its profile, which is usually achieved by rotating the crystal around one axis (here φ) while collecting data over a sequence of angle ranges $\varphi \rightarrow \varphi + \Delta\varphi$ as individual diffraction images. In traditional pump-probe experiments, each measurement is taken at a centre-time t relative to the start of the cycle, and the entire experiment is repeated for several t over the complete t_{cyc}. With delays of milliseconds and longer, a full time-resolved experiment collecting sufficient quality data for several t easily requires several hours, which is especially problematic for crystals that degrade with repeated light and/or X-ray exposure.

To address this, we implemented a "pump-multiprobe" strategy where data for all required t are obtained in one collection (Figures 1(d)/(e)). During each cycle the crystal is rotated forwards and backwards multiple times through the same $\Delta\varphi$, sampling the same angular range at multiple t, and an electronically-gated Pilatus 300K detector is used to collect each $\Delta\varphi$-sweep as a separate diffraction image. The acquisition time t_{acq} for each image is determined by the gate length and diffractometer rotation speed and dictates the time-resolution, here defined as the time over which each 3D structure is averaged. During each subsequent t_{cyc} the crystal is moved through the next angular range and data again collected for all t, and the process repeated to build-up a 180° φ-scan. This multi-oscillation approach reduces the time needed to collect a complete set of time-resolved datasets to <120 min, far more time-efficient than a conventional pump-probe experiment.

We also implemented automated, on-the-fly data-processing to enable rapid analysis. The diffraction images are sorted by t as they are recorded and, once all experiments are complete, datasets are indexed, integrated and solved automatically. A full sequence of 3D structure snapshots are thus obtained over the cycle, each averaged over t_{acq}. Once

an initial model for the structures is obtained, this can be included in the processing pipeline so that the data is automatically refined to extract the ES populations from each snapshot.

Experiment design. The pump-multiprobe strategy was used to examine the time-dependent ES population in **1** over a range of timescales. The experimental conditions required to match the ES lifetime to the intended measurement timescales were determined using numerical simulations[30] parameterised with excitation and decay kinetic measurements, and ES populations under continuous irradiation, all measured using conventional SCXRD (Extended Data §4). These simulations allowed us to select a t_{cyc} and optimise the t_{exc}, t_{dec} and measurement temperature to maximise the ES/GS ratio, enabling precise, targeted design of the pump-multiprobe experiments. We selected five t_{cyc} from 14-170 s with t_{acq} from 400 ms to 8 s (Table 1). The simulations suggested a temperature range of 260-290 K, which is above the 255 K ceiling for our previous decay kinetics measurements using conventional SCXRD methods.[30]

ES population dynamics on sub-second timescales. A total of 12 experiments were performed over the five t_{cyc}, each using a new crystal. By optimising the sequence timings and measurement temperatures, we obtained maximum ES conversions α_{max} of 33.7% (t_{acq} = 8 s), 21.3% (t_{acq} = 4 s), 10.7% (t_{acq} = 1.6 s), 11.8% (t_{acq} = 800 ms), and 10.4% (t_{acq} = 400 ms). Full α_{max} data for all 12 experiments are given in Table S16. After fitting, the refined populations were found to be within 68-98% (mean 84%) of the predicted maximum steady-state ES population α_{SS} achievable under continuous illumination at each experiment temperature (Table S19). This indicates that we obtain photoconversion levels approaching the theoretical maximum in most crystals.

The ES conversion is influenced by a number of factors including crystal size and shape,[30] and we thus observed some variation in the ES fractions obtained under similar conditions. In all cases, however, the α_{max} obtained with our LED set-up are a significant improvement on the few % reported for traditional laser-pump-X-ray-probe studies.[14-17, 27]

Each LED-pump-X-ray-multiprobe experiment yields a series of 3D structures spanning the excitation and decay periods. Good-quality structure refinements could be achieved with all datasets, with residual factors of R_{int} = 9.16-9.85 % (mean 9.55 %) and R_1 = 6.24-6.41 % (mean 6.32 %) across the 9 structures collected at the shortest t_{acq}. Table S17 provides full data for selected structures across all 12 pump-multiprobe experiments.

The fractional occupation of GS and ES isomers for each structure are refined using a standard disorder model, allowing the evolution of the ES population $\alpha(t)$ to be followed. We define the conversion fraction $\Delta\alpha(t) = \alpha(t) - \alpha(t = 0)$ as the percentage of molecules that are converted to the ES isomer at a time t. Figure 2 shows the behaviour in experiments with increasingly faster t_{cyc} and shorter t_{acq}, where in each case the temperature was optimised to ensure

near-complete ES decay. The same behaviour is seen in all experiments, suggesting the same fundamental isomerisation mechanisms at all the timescales/temperatures studied.

To investigate this further, we assume competing, independent excitation and decay processes, each described by the Johnson-Mehl-Avrami-Kolmogorov model,[30] and use numerical simulations to fit excitation and decay rates. Figure 2 confirms this model reproduces the measured data well, providing confidence in the fitted parameters. Fitted parameters for all pump-multiprobe experiments are given in Figures S17-S28, Table S18. At low temperature, the decay rate follows the Arrhenius law.[30] Figure 3 shows an Arrhenius analysis including low- and mid-temperature rate constants obtained from conventional SCXRD measurements, and high-temperature rate constants from the pump-multiprobe experiments. Both datasets fit the same trendline, providing strong evidence that the decay follows the same mechanism over a wide temperature range. We extract an activation energy E_A of 61.7 kJ mol^{-1} and an attempt frequency A of 48.3 GHz.

Finally, we note that we do not observe complete ES decay during the experiments. Since the decay is exponential, we adjusted t_{dec} to 4-5× the predicted kinetic $t_{1/2}$ at the measurement temperature to balance complete decay to a "clean" GS against a reasonable t_{cyc}. Despite this, we observed a low-level background excitation $\alpha(t = 0)$ of ~4 %, which we ascribe to a small but measurable level of X-ray excitation. While the α_{max} levels we measure have sufficient range to follow the excitation behaviour clearly, this finding has implications for the low excitation levels observed in traditional laser-pump-probe experiments.

Evolution of the electron density: molecular movies. The information provided by the pump-multiprobe measurements also allows us to visualise the changes in electron density on photoexcitation. This is achieved by generating Fourier electron-density difference maps (photo-difference maps) between the GS structure model at $t = 0$ and ES data recorded during the pump-multiprobe cycle. Figure 4 shows a series of photo-difference maps generated from an experiment at 265 K with t_{cyc} = 170 s, t_{exc} = 55 s, t_{dec} = 115 s, t_{acq} = 8 s and maximum $\Delta\alpha(t)$ = 33.7 %. Positive/negative residual peaks indicate regions where electron-density accumulates/depletes on excitation, showing the movement of atoms during the isomerisation.

The time-resolved snapshots can be combined to create a molecular movie showing the nitro↔nitrito conversion. We find that shorter time-resolutions decrease the quality of the photo-difference maps due to spurious ripples in the difference density, which we attribute to the reduced diffraction intensity due to X-ray flux limitations at shorter t_{acq} (although we emphasise that this data is still sufficient for good-quality structure solution).

Future developments: improved time-resolution with continuous readout using the Timepix3 detector chip. The practical limit on the number of time-delays and the t_{acq} in our pump-multiprobe experiment are determined by three variables: (1) the X-ray flux; (2) the "dead-time" needed to move the diffractometer between t_{acq}; and (3) the detector read-out time. At 400 ms we only require 5 % of the available beam, so modern synchrotron sources are easily capable of higher time-resolution. The dead-time for diffractometer movement can be minimised through alternative data-collection strategies. However, the 3 ms read-out of the Pilatus 300 K becomes limiting at ~10 ms and faster. This can be addressed using purpose-built time-resolved detectors such as those based on the Timepix3 hybrid active-pixel detector chip.[31] The Timepix3 detects and timestamps X-ray photons with an accuracy of 25 ns and outputs a continuous data-stream containing the 2D position, time of arrival (ToA) and time over threshold (ToT) of each photon event. This continuous data-stream eliminates read-out time and allows t_{acq} to be adjusted after collection, meaning that the experiment need not be constrained by having to choose a target time-resolution before data-collection.

To demonstrate the potential of our method to harness this technology, we performed proof-of-concept experiments using a single-module Timepix3 detector being developed at Diamond Light Source. The 1.98 cm^2 detector area was sufficient only to follow a single reflection, so we used our pump-multiprobe datasets to identify the (-2 1 0) reflection as tracking the ES population. We then ran a series of pump-probe experiments using similar timing sequences to the full SCXRD measurements, while recording continuously with the Timepix3 chip.

Figure 5(a) shows the intensity changes over a representative pump-multiprobe cycle. These are an excellent qualitative match to the refined ES population behaviour from full SCXRD experiments. Figures 5(b)/(c) show the results of repeated pump-multiprobe cycles and show that, while at shorter t_{exc} the maximum intensity is relatively consistent between cycles, for longer t_{exc} the effects of the photobleaching are clearly evident. Qualitative information on NO_2↔ONO switching can therefore be quickly determined using this method. However, we found that data-fitting did not yield quantitative kinetic information comparable to the full SCXRD experiments, which highlights the importance of our method in providing unambiguous 3D structure information at all time-points. The continuing development of larger-area Tristan 1M/10M Timepix3 detectors at Diamond will soon enable collection of complete SCXRD data, and the flexibility of not requiring a fixed t_{acq} may allow our method to access finer time-resolution.

Discussion

The novel pump-multiprobe methodology presented here leverages the advances in photon-counting detectors to study solid-state processes at second-to-millisecond timescales, with numerous benefits over existing pump-probe methods used for faster processes. Our method yields a complete set of high-quality SCXRD datasets averaged over sub-second

timescales, allowing the 3D structures of light-activated species to be determined without prior knowledge. By taking full advantage of the slower timescales, our method represents a powerful technique for following the population dynamics of ES species to obtain kinetic and mechanistic information, and can be utilised to unambiguously identify short-lived intermediate species by visualising changes in the electron density through creating photo-difference maps.

The pump-multiprobe method records data across multiple time-delays in each pump-probe cycle, which substantially shortens the experiment compared to previously-developed approaches and ensures that measurements at different time-delays are not unequally affected by cumulative crystal damage, photobleaching and/or X-ray excitation. The shorter overall experiment time helps to minimise these issues and, where they do occur, the experiment design means that all time-delays are affected equally and thus remain comparable.

The use of a pulsed-LED pump, rather than a laser, also sets our method apart from existing pump-probe experiments. Provided an LED pump can deliver sufficient power, it can be built with low-cost components to provide a variety of wavelength/power profiles and allows complete control over the timing sequence and illumination direction, while coverage can be optimised without complex alignment, optics and safety protocols. An LED pump also spreads the irradiation energy load in time, minimising unwanted effects such as heating and potentially yielding higher overall photoexcitation in crystals like **1**, where the excitation and decay are in equilibrium. The flexibility of this setup allows the same experiment to study a range of light-induced phenomena at timescales from minutes to microseconds, depending on the LED components used. On the other hand, designing, commissioning, and maintaining a laser setup with similar flexibility would be very resource intensive. We note that laser diodes capable of pulses down to a few hundred picoseconds are also available.[32]

In linkage isomers like **1**, the maximum achievable photoexcitation at a given temperature will always be limited by the competing thermal decay to the steady-state occupation achieved under continuous illumination.[30] While a short burst of high-intensity photons might produce a non-equilibrium population for a short period of time, the low conversion fractions typically seen following laser excitation suggests this does not happen efficiently in practice. Indeed, our previous work with **1** showed that the conversion saturates beyond a certain brightness, indicating a threshold beyond which excess photons are either not absorbed,[30] or, worse, converted to heat to elevate the decay rate. Even using the LED pump, we observed gradual bleaching during our experiments and this would likely be a larger issue with lasers delivering comparable or higher powers over much shorter pulse-widths. There is a clear need for more systematic investigation of these problems and their implications for pump-probe experiments.

Finally, the observation of spurious peaks in the photo-difference maps at shorter t_{acq} highlight that the experiment remains diffraction-limited and the signal-to-noise ratio needs to be improved for faster timescales. For **1**, this

is not a limitation of the X-ray source but is necessary to avoid X-ray-induced excitation at higher flux. This is likely to be a problem for many crystal systems and motivates the development of faster and more sensitive detector technologies. In this vein, the flexibility afforded by moving away from traditional imaging to event-counting detectors, such as the Timepix3 chip explored in this work, will be crucial for future time-resolved SCXRD studies at shorter timescales.

Online Methods

Test crystal. 1 crystallises as a tetrahydrofuran solvate in the monoclinic space group $P2_1/n$ with one cation, one BPh_4 counter-anion and one THF molecule per asymmetric unit (Figure S1, Extended Data). The photoactive $[Pd(Bu_4dien)(NO_2)]^+$ cation excites from a ground-state (GS) nitro (η^1-NO_2) to an excited-state (ES) *endo*-nitrito (η^1-ONO) isomer in the single-crystal with 100 % conversion by irradiating at $\lambda \approx 400$ nm.[29] The reverse ONO → NO_2 process is thermally activated with a measured activation energy E_A of 51.6-60.3 kJ mol^{-1}.[30] Complete GS → ES excitation has a minimal effect on the surrounding crystal structure, with a small 0.14 % expansion of the lattice at 100 K and negligible loss of diffraction over repeated transformations.[29] Crucially for the present work, the ES lifetime is strongly temperature-dependent, with a continuous variation in the kinetic half-life over seven orders of magnitude from ~10^7 s (115 days) at 180 K and 1 s at room temperature.[30] Full crystal data and images for **1** are provided in the Extended Data.

Excitation source. The light pump in our experiments is a pulsed LED array incorporating 18 round 3 mm LEDs (Bivar UV3TZ-400-30) mounted into a part-spherical holder to point directly at the crystal (Figure 1a). This custom 3D-printed LED sphere can hold up to 25 round (T-1) 3mm through-hole LEDs, with all diodes pointing directly at the sample position. The LEDs are connected *via* an Adafruit TB6612 driver (Figure S2) to a standard laboratory DC power supply (ISO-TECH IPS303DD). The driver powers the LED array in response to a 3.3V TTL signal from a timeframe generator (TFG2), enabling synchronisation between the array and diffractometer through the beamline's Generic Data Acquisition (GDA) software[33] as outlined in the following section. The timing of the LED circuit is monitored through a Tektronix TDS3012B oscilloscope. A circuit diagram for the set-up is included in the Extended Data (Figure S2).

The array is mounted directly below the sample with a crystal-to-LED distance of 9.57 cm (Figure 1b) and illuminates the crystal without impeding the X-ray beam path or restricting the detector position at any point during the experiment. Rotation of the crystal about φ during the LED pulses further ensures uniform illumination. The light power at the crystal was measured to be 23 mW (Extended Data, §2(ii)). The LED rise and fall times were tested and found to be negligible on the timescale of the experiment, and pulse separation down to ~200 μs could be achieved (Extended Data, §2(iii)). Reliable pulse trains with microsecond and shorter repetition rates could likely be obtained using alternative LEDs or laser diode components.

The LED light pump is synchronised to the diffractometer hardware using the GDA software.[33] Simple electronic triggering provides complete control over the excitation pulse length t_{exc}, allowing us to optimise the excitation and improve substantially on the 1 - 3 % photoexcitation levels typically achieved in single-crystal studies using short laser pulses.[14-17] The length of the decay period, the complete cycle time, and the acquisition period (t_{dec}, t_{cyc} and t_{acq},

respectively) are also flexible, within the limits of the diffractometer, and the timing sequence can be implemented using relatively inexpensive electronics. Further details of the experimental setup are provided in the Extended Data.

Sample excitation tests. We first carried out test experiments to determine whether prolonged exposure to LED light and/or synchrotron X-rays could lead to unfavourable changes in the sample, e.g. crystal degradation or X-ray induced excitation. Full details are provided in the Extended Data (§3). Though no appreciable crystal degradation was observed in the X-ray tests, a steady increase in the ES nitrito-ONO isomer occupancy was measured with increasing exposure time. This X-ray induced excitation could be limited by increasing the attenuation of the synchrotron beam, leading us to select a 5 % beam intensity for experiments, which produced a baseline X-ray excitation of *c.a.* 3 % in testing. LED exposure tests revealed that prolonged irradiation for *c.a.* 4 h led to irreversible damage at the crystal surface, causing a visible colour change from pale-yellow to orange, alongside gradual photobleaching with time (Figure S7). To minimise the influence of these effects, a new crystal was used for each experiment.

Pump-multiprobe synchronisation. Data were collected using an XPS four-circle diffractometer equipped with a Pilatus 300K detector and an Oxford Cryosystems Cryostream 7 liquid-nitrogen cooling device for temperature control. The GDA software, which functions as the user interface for setting up data collections on beamline I19 at Diamond Light Source, was used to implement the pump-multiprobe synchronisation. The GDA interfaces with the diffractometer control software, EPICS,[34] to set the start and end points for the φ scans, the scan velocity and to set up the detector for collecting images. The "position compare" TTL output on the diffractometer, which goes high while the φ-axis is swept over the desired angle range, is used as the master signal to trigger the detector and, *via* the GDA and TFG2 timeframe generator, the LED driver. The jitter in the response of the TFG2 and Pilatus 300 K are 1.5625 and 10 ns, respectively, and completely negligible on the timescale of our experiments. Experiment metadata, including the diffractometer positions, detector responses and LED switching, are logged with timestamps to monitor the synchronisation. A schematic representation of the pump-multiprobe synchronisation is available in the Extended Data (Figure S29).

Pump-multiprobe data-collection strategy. In order to maximise coverage of reciprocal space whilst minimising the "downtime" due to diffractometer movement between data-collection positions, we devised a collection strategy based on scanning the phi (φ)-axis. A target pump-probe cycle time t_{cyc} is chosen and numerical simulations are used to optimise the excitation pulse length t_{exc}, decay period t_{dec} and measurement temperature T to maximise the difference between the ES populations $\alpha(t)$ at the start of the cycle ($t = 0$) and after the pump pulse ($t = t_{\mathrm{exc}}$). We then

select an acquisition time t_{acq}, and an appropriate scan width $\Delta\varphi$ and rotation speed are determined. There is a small time delay between acquisition periods while the diffractometer motors are reversed, and the synchronisation between the pump, diffractometer and detector requires an integral number of acquisitions in each of the excitation and decay periods. The chosen t_{cyc}, t_{exc}, t_{dec} and t_{acq}, together with information from the simulations, thus also determines the number of probe measurements per cycle.

To obtain a good quality, complete set of single-crystal X-ray data at each t, a sufficient number of φ scans must be collected to cover the reciprocal space of the crystal. This is achieved by performing two 180 ° φ scans at ω = – 90 °, κ = 0 °, 2θ = 12 ° (scan 1) and ω = – 90 °, κ = 60 °, 2θ = 12 ° (scan 2). Δφ must be chosen carefully to balance fast data collection and a short overall experiment duration with recording accurate diffraction intensities by sampling reflections multiple times across their profile. The φ-axis rotation speed was 2 ° / s. To minimise the time overhead of moving the diffractometer axes, we perform both forwards and reverse φ scans and require an odd number of probe measurements so that the diffractometer ends each pump-probe cycle in the correct start position for the following scan (c.f. Figure 1). The Δφ and timings used in the experiments in this work are listed in Table 1.

As an example, with a target t_{cyc} = 170 s, the simulations predict t_{exc} = 52.7 s, t_{dec} = 117.3 s and a measurement temperature of 260 K. We select a t_{acq} of 8 s, for which an appropriate $\Delta\varphi$ is 16 ° with a φ-axis rotation speed of 2 ° / s. Including overheads, we obtain 9.6 s per time delay, allowing for a total of 17 Δt within the 170 s t_{cyc}. The t_{exc} and t_{dec} are adjusted to 55 and 115 s to include an integral number of probe measurements, giving 5 and 12 Δt during the excitation and decay periods, respectively. The diffractometer φ-axis will therefore scan the same angle range Δφ 17 times during each cycle. Each φ scan covers 180 °, so a total of 11 complete pump-multiprobe cycles are recorded for a full scan, and 22 cycles across the complete experiment (i.e. 11 complete cycles for each of the two φ scans with the ω, κ and 2θ positions given above).

Data-processing. Once the data collection has begun, the automated processing procedures can be started in parallel.[35]

The diffraction images are sorted on-the-fly during the data collection into separate directories for each delay time t recorded. This ensures that the diffraction images are in the correct format for routine SCXRD processing. Automated data indexing and integration are performed by DIALS,[36] while data scaling and absorption correction are applied by AIMLESS,[37] all of which are run through the xia2 interface. Initial structure refinement is also performed automatically by running the processed data through SHELXL and importing a model solution containing both the GS nitro-(η^1-NO_2) and ES nitrito-(η^1-ONO) isomers as a standard disorder model that utilises SHELX PART instructions to refine the GS:ES

isomer occupancy ratio (and therefore the conversion fraction) as a free variable. Once the refinement has converged, the conversion fraction is extracted from the resulting SHELX CIF file, and the conversion fractions for all t are tabulated in a separate text file. This enables a rapid initial assessment of the pump-multiprobe experiment results and hence fast decision-making with regards to adjusting variables such as the temperature. For each dataset, complete automated data processing takes *c.a.* 15 minutes to complete and requires no user intervention. We take advantage of the Diamond Light Source computing cluster, enabling us to process all of the datasets from a pump-multiprobe experiment simultaneously on different cluster nodes, so that the number of t recorded does not affect the overall data-processing time.

To finalise the crystal structures and confirm the presence and occupancy of the photo-induced ES isomer, the data were later analysed manually using Olex2.[38] This manual processing was performed to ensure data were suitable for publication, but in practice we found that the automatic data processing generated structures that closely resembled the final versions prepared manually. Structure solution was performed using dual-space methods with SHELXT, and structures were subsequently refined by full matrix least squares against F^2 with SHELXL. Hydrogen atoms were positioned geometrically and refined using a riding model. The hydrogen atom isotropic displacement parameters were fixed to U_{iso}(H) = 1.5 × (for CH_3) or U_{iso}(H) 1.2 × (for CH_2 and CH). ES population conversion fractions $\alpha(t)$ for all structures were refined directly from the data using a standard disorder model for the partially-isomerised nitrite ligand, utilising SHELX PART instructions as outlined above.

Fourier electron-density difference maps between the GS and photo-excited models were generated by refining the GS structure (atomic coordinates and anisotropic displacement parameters) against the photo-excited reflection file (HKL file) with SHELXL. The GS parameters were prevented from changing significantly by using a DAMP 20000 instruction, and a LIST 3 instruction was chosen to output the correct FCF file required to generate the photo-difference maps. Photo-difference maps were plotted using the Maps tool in Olex2,[38] and individual images for each t were generated and combined into molecular movies using the ImageMagick software.[39]

Kinetic modelling and data fitting. Previous work on this and other nitrite linkage isomers has shown that the GS → ES excitation and reverse ES → GS decay processes are well described by the Johnson-Mehl-Avrami-Kolmogorov (JMAK) model:

$$\alpha(t) = \alpha_\infty + (\alpha_0 - \alpha_\infty)\exp[-kt^n]$$

where α is the fractional population of the growing phase, α_0 and α_∞ are the initial and final populations respectively, k is the rate constant for the transformation and the Avrami exponent n is related to the dimensionality D of the growth by $D = n - 1$.[40-43]

The decay rate is temperature dependent and can be described by an Arrhenius law with an activation energy E_A and an attempt frequency A:

$$k(T) = A\exp[-E_\mathrm{A}/RT]$$

Using a two-process model with competing, independent, excitation and decay processes, we developed a simple numerical simulation tool to predict the time evolution of the ES population under a variety of experimental conditions including simulated pump-probe sequences.[30] As implemented, our model required five parameters, the rate constant k_exc and Avrami exponent n_exc for the excitation process (assumed to be temperature independent), and the Arrhenius parameters $E_\mathrm{A,dec}/A_\mathrm{dec}$ and Avrami exponent n_dec for the decay. The Avrami exponents were fixed to an integer value of 1 based on previous work.[30] To predict the optimum conditions for the time-resolved measurements, the model was parameterised against three sets of pre-experiments, *viz.* (1) excitation measurements at 150 K; (2) decay measurements from 240-260 K; and (3) steady-state measurements under continuous illumination from 250-300 K. The simulations then allowed us to select an appropriate temperature and excitation and decay times for a given target cycle time with a typical accuracy of ~10 K.

We also used the simulation tool to fit the measured pump-probe data and extract rate constants for the excitation and decay processes (the Avrami exponents n_exc for both processes were again fixed to unity). Full details of the pre-experiments, modelling and data fitting are given in the Extended Data (§4 and 6).

Timepix3 single-reflection experiments, data processing and data fitting. Proof-of-concept measurements were performed using a single-module Timepix3-based detector to follow the (-2 1 0) reflection, which was found to show a large increase in intensity between the GS and ES structures.

The raw output from the Timepix3 chip is a data stream containing the position, time of arrival (ToA) and time over threshold (ToT) value for each detected photon. This data stream was synchronised to the timing electronics to record additional timestamped events marking the start and end of each pump-probe sequence. After collecting for a fixed time, the photon capture events are rebased to the pump-probe cycle time, a region of interest (RoI) containing the reflection is defined together with a nominal t_acq, which we chose to be 50 ms to provide a suitable number of intensity-sampling points

across pump-multiprobe cycle periods of a few seconds in duration, and the intensity (photon counts, number of events) in the RoI is binned into time windows of length t_{acq}.

A script was used to automatically extract the photon count data from the Timepix3 data stream files and produce histogram plots of the reflection intensity as a function of irradiation and experiment time, as shown in Figure 5.

Supplementary information

Supplementary Figures S1 – S30 and supplementary Tables S1 – 18 are provided as a PDF.

Data-Access statement

Raw data and codes used for data collection, processing and analysis can be obtained from the authors on reasonable request. CIF files for all 178 structures collected are available from the Cambridge Structural Database, deposition numbers: 2127495–2127511, 2127514–2127530, 2127548–2127564, 2127565–2127583, 2127724–2127742, 2127809–2127827, 2127832–2127850, 2128443–2128453, 2128633–2128645, 2128661–2128669, 2128671–2128679, 2132660–2132668.

Coding availability statement

Single crystal X-ray data were collected using the open-source Diamond Light Source General Data Acquisition (GDA) software, for which further access information is available at www.opengda.org. Single crystal X-ray data were indexed, integrated and scaled using the open source xia2 software (https://github.com/xia2/xia2), and solved and refined using the ShelXT and ShelXL software (https://shelx.uni-goettingen.de; free for academic and non-for-profit users). The code for performing the kinetic analyses and numerical simulations is available on GitHub at https://github.com/JMSkelton/Linkage-Isomer-JMAK-Kinetics. This code makes use of the Python 3 programming language (https://www.python.org) with the NumPy and SciPy packages (https://numpy.org, https://scipy.org) as well as our FitLib package (https://github.com/skelton-group/FitLib), all of which are open source and freely available.

Acknowledgements

The authors thank Diamond Light Source for the award of synchrotron beamtime in visits MT17306-1, MT17306-2 and CM19670-3. PRR, LEH, JS and AP are grateful to the EPSRC for support (EP/K004956/1). LEH is current supported by

a Royal Society University Research Fellowship (URF\R1\191104). JS is currently supported by a UKRI Future Leaders Fellowship (MR/T043121/1) and previously held a University of Manchester Presidential Fellowship.

Author contributions

Time-resolved X-ray data were collected by L.E.H., P.R.R., M.R.W., J.M.S., A.R.P., L.K.S. and D.R.A. at Diamond Light Source. J.M.S. developed numerical simulations for experiment design and data fitting, and M.R.W. designed the experiment protocols. L.E.H. processed and analysed all SCXRD datasets, prepared X-ray data for publication and produced photodifference maps and molecular movies. P.H. G.C., D.O. and B.H.W. developed the Timepix3 detector setup and associated software, and performed time-resolved data collections with M.R.W. and L.E.H. L.E.H, P.R.R., J.M.S. and C.C.W. wrote the manuscript, with input from all authors.

Competing interests

The authors declare no competing interests.

References

1. Coppens, P., Fomitchev, D.V., Carducci, M.D. & Culp, K. Crystallography of molecular excited states. Transition-metal nitrosyl complexes and the study of transient species. *Dalton Trans*., 865-872 (1998).

2. Coppens, P. The dramatic development of X-ray photocrystallography over the past six decades. *Struct. Dyn.* **4**, 032102-032102 (2017).

3. Hatcher, L.E. & Raithby, P.R. Dynamic single-crystal diffraction studies using synchrotron radiation. *Coord. Chem. Rev*. **277–278**, 69-79 (2014).

4. Cole, J.M. A new form of analytical chemistry: distinguishing the molecular structure of photo-induced states from ground-states. *Analyst* **136**, 448-455 (2011).

5. Pandey, S. *et al.* Time-resolved serial femtosecond crystallography at the European XFEL. *Nat. Methods* **17**, 73-78 (2020).

6. Pearson, A.R. & Mehrabi, P. Serial synchrotron crystallography for time-resolved structural biology. *Curr. Opin. Struct. Biol.* **65**, 168-174 (2020).

7. Moffat, K. The frontiers of time-resolved macromolecular crystallography: movies and chirped X-ray pulses. *Faraday Discuss.* **122**, 65-77 (2003).

8. Badali, D.S. & Miller, R.J.D. Robust reconstruction of time-resolved diffraction from ultrafast streak cameras. *Struct. Dyn.* **4**, 054302 (2017).

9. Miller, R.J.D. Femtosecond Crystallography with Ultrabright Electrons and X-rays: Capturing Chemistry in Action. *Science* **343**, 1108 (2014).

10. Hough, M.A. & Owen, R.L. Serial synchrotron and XFEL crystallography for studies of metalloprotein catalysis. *Curr. Opin. Struct. Biol.* **71**, 232-238 (2021).

11. Jarzembska, K.N. *et al.* Shedding Light on the Photochemistry of Coinage-Metal Phosphorescent Materials: A Time-Resolved Laue Diffraction Study of an AgI–CuI Tetranuclear Complex. *Inorg. Chem.* **53**, 10594-10601 (2014).

12. Makal, A. *et al.* The development of Laue techniques for single-pulse diffraction of chemical complexes: time-resolved Laue diffraction on a binuclear rhodium metal-organic complex. *Acta Cryst. A* **67**, 319-326 (2011).

13. Deresz, K.A., Łaski, P., Kamiński, R. & Jarzembska, K.N. Advances in Diffraction Studies of Light-Induced Transient Species in Molecular Crystals and Selected Complementary Techniques. *Crystals* **11**, 1345 (2021).

14. Vorontsov, I.I. *et al.* Capturing and Analyzing the Excited-State Structure of a Cu(I) Phenanthroline Complex by Time-Resolved Diffraction and Theoretical Calculations. *J. Am. Chem. Soc.* **131**, 6566-6573 (2009).

15. Coppens, P. *et al.* A very large Rh-Rh bond shortening on excitation of the [Rh2(1,8-diisocyano-p-menthane)4]2+ ion by time-resolved synchrotron X-ray diffraction. *Chem. Commun*. 2144-2145 (2004).

16. Kim Christopher, D., Pillet, S., Wu, G., Fullagar Wilfred, K. & Coppens, P. Excited-state structure by time-resolved X-ray diffraction. *Acta Cryst. A* **58**, 133-137 (2002).

17. Collet, E. *et al.* 100 Picosecond Diffraction Catches Structural Transients of Laser-Pulse Triggered Switching in a Spin-Crossover Crystal. *Chem. - Eur. J.* **18**, 2051-2055, S2051/2051 (2012).

18. Azzolina, G. *et al.* Single Laser Shot Photoinduced Phase Transition of Rubidium Manganese Hexacyanoferrate Investigated by X-ray Diffraction. *Eur. J. Inorg. Chem.* 3142-3147 (2019).

19. Garman, E.F. & Weik, M. Radiation Damage in Macromolecular Crystallography, in Methods in Molecular Biology, Vol. 1607. Humana Press, New York, NY, USA (2017).

20. Teng, T.-y. & Moffat, K. Primary radiation damage of protein crystals by an intense synchrotron X-ray beam. *J. Synchrotron Radiat.* **7**, 313-317 (2000).

21. Poneti, G. *et al.* Soft-X-ray-Induced Redox Isomerism in a Cobalt Dioxolene Complex. *Angew. Chem. Int. Ed.* **49**, 1954-1957 (2010).

22. Papanikolaou, D. *et al.* X-ray Illumination Induced Fe(II) Spin Crossover in the Prussian Blue Analogue Cesium Iron Hexacyanochromate. *J. Am. Chem. Soc.* **128**, 8358-8363 (2006).

23. Garman, E.F. & Weik, M. X-ray radiation damage to biological macromolecules: further insights. *J. Synchrotron Radiat.* **24**, 1-6 (2017).

24. Lignos, I., Stavrakis, S., Kilaj, A. & deMello, A.J. Millisecond-Timescale Monitoring of PbS Nanoparticle Nucleation and Growth Using Droplet-Based Microfluidics. *Small* **11**, 4009-4017 (2015).

25. Christensen, J. *et al.* Radiation damage in small-molecule crystallography: fact not fiction. *IUCrJ* **6**, 703-713 (2019).

26. Milo, R., Phillips, R. & Orme, N. Cell Biology by the Numbers. Garland Science, New York, NY, USA (2016).

27. Casaretto, N. *et al.* In-house time-resolved photocrystallography on the millisecond timescale using a gated X-ray hybrid pixel area detector. *Acta Cryst. B.* **73**, 696-707 (2017).

28. Yorke, B.A., Beddard, G.S., Owen, R.L. & Pearson, A.R. Time-resolved crystallography using the Hadamard transform. *Nat. Methods* **11**, 1131-1134 (2014).

29. Hatcher, L.E. Raising the (metastable) bar: 100% photo-switching in $[Pd(Bu4dien)(\eta^1\text{-}\underline{N}O_2)]^+$ approaches ambient temperature. *CrystEngComm* **18**, 4180-4187 (2016).

30. Hatcher, L.E. *et al.* Monitoring photo-induced population dynamics in metastable linkage isomer crystals: a crystallographic kinetic study of $[Pd(Bu_4dien)NO_2]BPh_4$. *Phys. Chem. Chem. Phys.* **20**, 5874-5886 (2018).

31. Poikela, T. *et al.* Timepix3: a 65K channel hybrid pixel readout chip with simultaneous ToA/ToT and sparse readout. *J. Instrum.* **9**, C05013-C05013 (2014).

32. Horiba, NanoLED Pulsed Laser and LED Light Sources, <https://www.horiba.com/en_en/products/detail/action/show/Product/nanoled-1384/> Accessed 04/01/2022.

33. Diamond General Data Aquisition (GDA) software, <http://www.opengda.org/> Accessed 04/01/2022.

34. Experimental Physics and Industrial Control System (EPICS), <https://epics.anl.gov/about.php> Accessed 04/01/2022.

35. Gerstel M., Ashton A., Gildea R.J., Levik K. & G. Winter. Data Analysis Infrastructure for Diamond Light Source Macromolecular & Chemical Crystallography and Beyond. *International Conference on Accelerator and Large Experimental Physics Control Systems (17th)*, New York, NY, USA (2019).

36. Winter, G. *et al.* DIALS: implementation and evaluation of a new integration package. *Acta Cryst. D.* **74**, 85-97 (2018).

37. Evans, P.R. & Murshudov, G.N. How good are my data and what is the resolution? *Acta Cryst. D.* **69**, 1204-1214 (2013).

38. Dolomanov, O.V., Bourhis, L.J., Gildea, R.J., Howard, J.A.K. & Puschmann, H. OLEX2: a complete structure solution, refinement and analysis program. *J. Appl. Cryst*. **42,** 339-341 (2009).

39. The ImageMagick Development Team. ImageMagick (2021). <https://imagemagick.org> Accessed 04/01/2021.

40. Avrami, M. Kinetics of Phase Change. III. Granulation, Phase Change, and Microstructure. *J. Chem. Phys.* **9**, 177-184 (1941).

41. Avrami, M. Kinetics of Phase Change. II. Transformation-Time Relations for Random Distribution of Nuclei. *J. Chem. Phys.* **8**, 212-224 (1940).

42. Avrami, M. Kinetics of Phase Change. I. General Theory. *J. Chem. Phys.* **7**, 1103-1112 (1939).

43. More, R. *et al.* Photodimerization of Crystalline 9-Anthracenecarboxylic Acid: A Nontopotactic Autocatalytic Transformation. *J. Phys. Chem. C* **114**, 4142-4148 (2010).

Table legends

Table 1 | Pump-probe sequences tested in this work. Each row lists the key parameters shown in Fig. 1, *viz.* the cycle time t_{cyc}, the excitation and decay times $t_{\mathrm{dec}}/t_{\mathrm{exc}}$, the φ-angle range Δφ the crystal is rotated through during each cycle, and the time-resolution t_{acq} of the measured X-ray structures.

Tables

t_{cyc} [s]	t_{exc} [s]	t_{dec} [s]	Δφ [deg]	t_{acq} [s]
170	55	115	1.6	8.0
108	35	73	8.0	4.0
35	14	21	3.2	1.6
22	8	14	1.6	0.8
14	5	9	0.8	0.4

Table 1

Figure legends

Figure 1 | Pump-probe SCXRD experiments using pulsed LEDs. (a)/(b) show a CAD drawing (a) and photograph (b) of the 3D-printed LED holder *in situ* on the diffractometer. (c)-(d) illustrate the data-collection procedure. The sample is subjected to repeated excitation/decay cycles of duration t_{cyc} (c). The LEDs are activated for t_{exc} to generate a photo-stationary excited-state (ES) population (yellow) then switched off for t_{dec} to allow the ES population to decay (blue). During each sequence the goniometer φ-axis is swept backward and forward through an angle range $\Delta\varphi$ (d) and the detector is electronically gated to record a series of data frames over a time interval t_{acq} (e). The start and end points of the φ sweep are incremented after each sequence, thereby obtaining a time series of complete φ scans sampling the excitation/decay curve with a resolution t_{acq}. The process is repeated to collect φ scans with the other goniometer axes in different positions to build up a full single-crystal dataset.

Figure 2 | Time-resolved pump-multiprobe single-crystal diffraction measurements on 1. The five plots show the time dependence of the ES population $\alpha(t)$ during successively shorter pump-multiprobe sequences where the temperature and excitation time are optimised to engineer similar kinetic behaviour. On each plot, the orange and blue shaded regions mark the excitation and decay parts of the sequence, respectively. The markers show the measured $\alpha(t)$, each refined from a full single-crystal X-ray data set averaged over the time t_{acq} indicated on each plot. The solid lines are fits of the data using numerical simulations with a two-process JMAK model with competing excitation and decay.

Figure 3 | Temperature dependence of the decay rate of the metastable isomer of 1. The plot shows an Arrhenius analysis of decay rate constants *k* obtained from three sets of measurements, *viz.* low- and mid-temperature photocrystallographic decay measurements, performed using a lab source (blue) and at the Diamond Light Source synchrotron facility (DLS - red), and high-temperature time-resolved measurements performed with our pump-multiprobe strategy (yellow). The black line is a fit to the Arrhenius law with the fitting parameters as shown. The low-temperature and some of the mid-temperature data are taken from our previous work.[30]

Figure 4 | Selected photo-difference maps illustrating the change in electron density in 1 during photoexcitation and decay at 265 K. Fourier electron-density difference maps calculated between the fixed GS coordinates and the ES structure data (ellipsoids shown at 50% probability). Green and red contours show regions of density accumulation and depletion,

respectively. (a)-(d) are from structures recorded during the LED illumination period t_{exc}, while (e)-(h) are from structures recorded during the ES decay period t_{dec}.

Figure 5 | Intensity of the (-2 1 0) reflection of 1 recorded using a Timepix3 detector chip. (a) Intensity change during one cycle with t_{exc} = 2 s (LEDs on) and t_{dec} = 5 s (LEDs off) at T = 286 K, averaged over eight repeats. (b) Intensity change over ten consecutive cycles with t_{exc} = 2 s and t_{dec} = 5 s at T = 286 K. (c) Intensity change over ten consecutive cycles with t_{exc} = 8 s and t_{dec} = 24 s at T = 280 K. In each case the photon events recorded by the detector are integrated into 50 ms time bins.

Figures

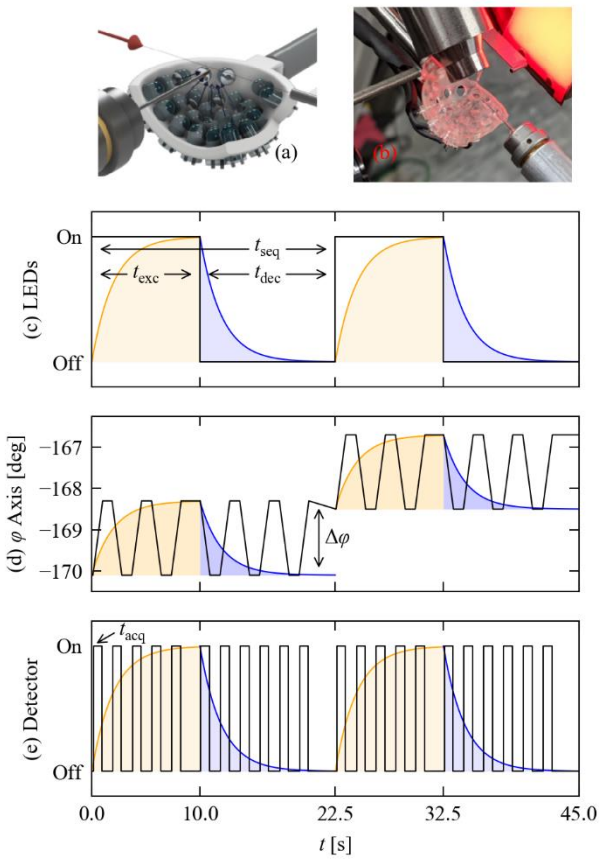

Figure 1

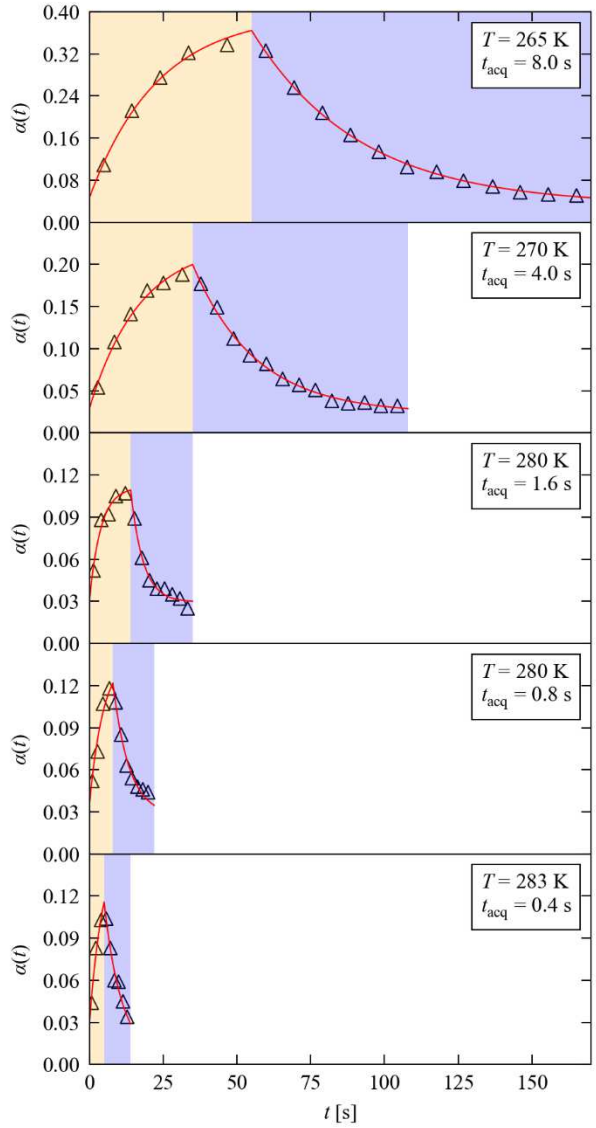
T = 265 K
t_acq = 8.0 s
T = 270 K
t_acq = 4.0 s
T = 280 K
t_acq = 1.6 s
T = 280 K
t_acq = 0.8 s
T = 283 K
t_acq = 0.4 s
α(t)
t [s]

Figure 2

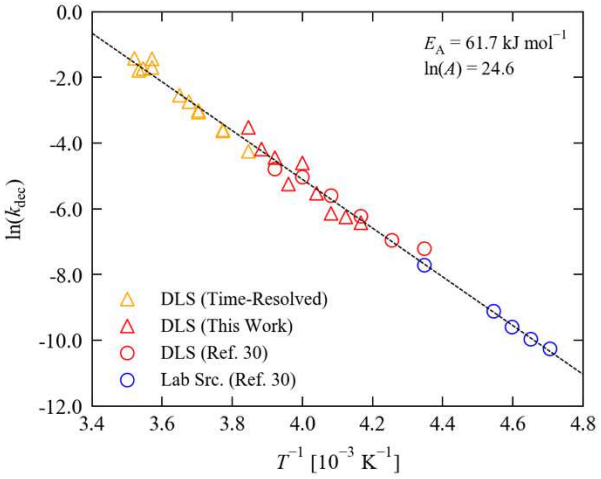

Figure 3

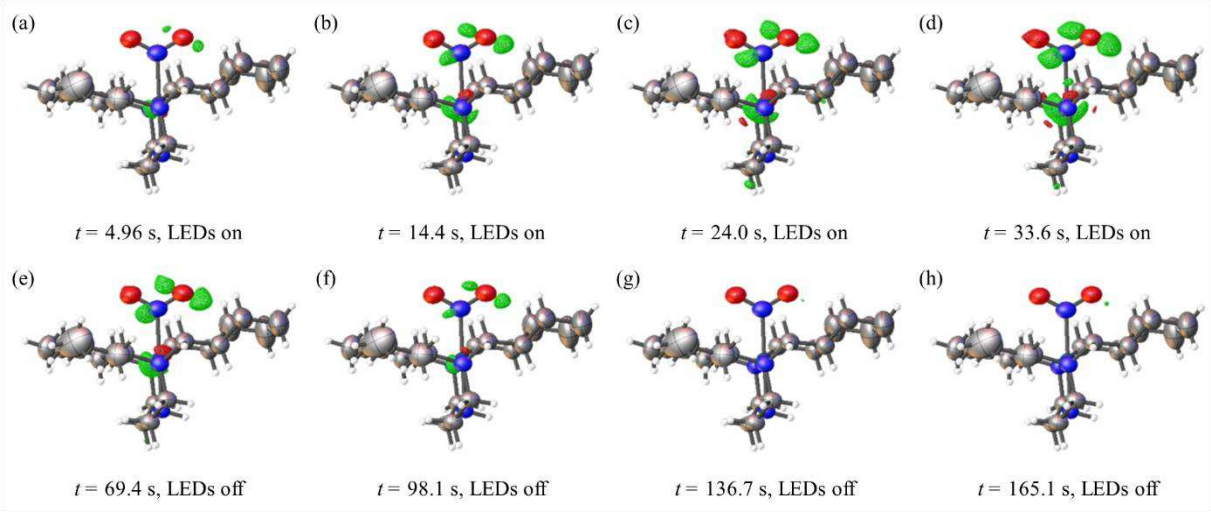

Figure 4

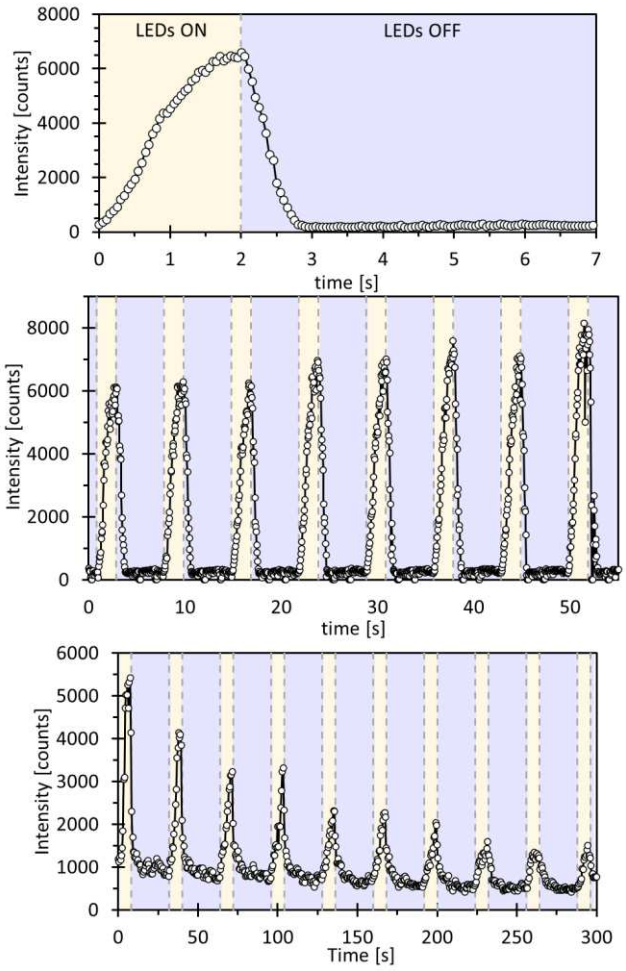
LEDs ON
LEDs OFF
Intensity [counts]
time [s]
Intensity [counts]
time [s]
Intensity [counts]
Time [s]

Figure 5

Supplementary Files

This is a list of supplementary files associated with this preprint. Click to download.

- ESI20220111.docx
- 16sAnimation.gif
- 04sAnimation.gif
- 08sAnimation.gif
- 4sAnimation.gif
- 8sAnimation.gif